Journal of Solid Mechanics and Materials Engineering

Vol. 2, No. 4, 2008

Full-Field Isoclinic Evaluation in Digital Phase-Shifting Photoelasticity Applied to C-Shaped Model*

Yudai NOMURA**, Pichet PINIT*** and Eisaku UMEZAKI**

**Nippon Institute of Technology

4-1 Gakuendai, Miyashiro, Saitama 345-8501, Japan

E-mail: umezaki@nit.ac.jp

***King Mongkut's University of Technology Thonburi

126 Prachautid, Bangmod, Thungkru, Bangkok 10140, Thailand

E-mail: ipichet@yahoo.com

Abstract

The full-filed evaluation of the isoclinic parameter in digital photoelasticity is presented. The proposed method is based on the four-step color phase shifting technique and the phase unwrapping (PU) algorithm. It is experimentally applied to an eccentrically loaded split ring (C-shaped model). Experimental results show that the isoclinic-angle map obtained is almost free from the influence of the isochromatic parameter and the isoclinic values lie in the physical range, $-\pi/2$ to $+\pi/2$, regardless of the presence of the isotropic point or region.

Key words: Digital Photoelasticity, Isoclinic Angle, Phase-Shifting Technique, Phase Unwrapping, True Range

1. Introduction

Based on the well-known phase-shifting technique (PST), two important problems arise when calculating ϕ: the isochromatic-isoclinic interaction [1] and the wrapped phase data. The first problem physically occurs because of the deviation of the isoclinic parameter at and near the isochromatic fringe skeleton. In case of the wrapped phase data, it arises because only unambiguous phase is known at most in the range of $(-\pi/4, +\pi/4]$ (modulo $+\pi/2$) instead of its true range of $(-\pi/2, +\pi/2]$ (modulo $+\pi$). Note that the symbol (a, b] represents $a < \phi \le b$. If this problem is still unsolved, the ambiguity exists on whether the map of isoclinic angle represents σ_1 or σ_2 direction over the entire domain and this effect propagates to the determination of the isochromatic parameter especially in case of using the circular polariscope.

Many efforts have been devoted to propose methods to automatically solve these problems [2-7]. These methods used either the plane or circular polariscope, and provided the isoclinic parameter both in the half of the true range [2-4], i.e. $[0, +\pi/2]$ and in the true range after unwrapping the wrapped phase data [5-7]. All methods work well with the problem of the circular disk under compression; however, they have not been designed for the problems or models having the isotropic point while the isotropic point is considered to be a main source that easily makes the PU unreliable.

The developed PU algorithm with capability of dealing with the problems having the isotropic point has been proposed [8]. In this work, the PU is applied to evaluate another photoelastic model having an isotropic region rather than point(s) in order to confirm its performance. The problem of the eccentrically loaded split ring (C-shaped model) is studied.

*Received 16 Nov., 2007 (No. 07-0728)
[DOI: 10.1299/jmmp.2.530]

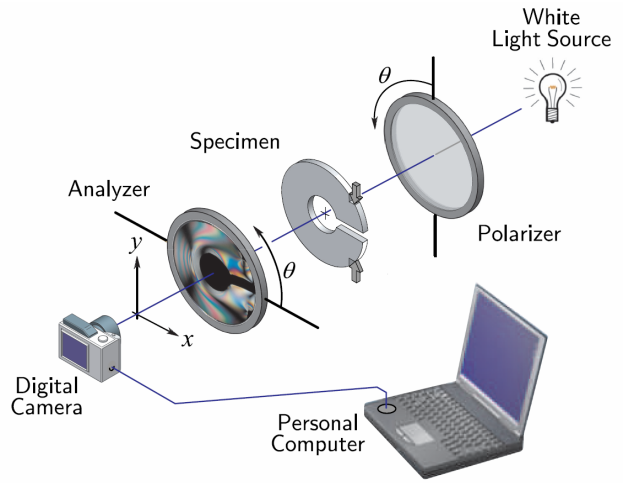

Fig. 1 Schematic of dark-field plane polariscope system used for collecting the photoelastic fringe images.

2. Evaluation of Isoclinic Parameter

2.1 Equation of isoclinic parameter

Consider the dark-field plane polariscope system with white light source where the reference axis is in horizontal (x-axis) (Fig. 1). When a photoelastic model is properly placed in the system and then loaded by a force, the general equation of the intensity I_λ coming out of the camera of a color imaging system with generic orientation m of a crossed fashion of the polarizer and analyzer can be expressed as [8]

$$I_{m,\lambda} = I_{\mathrm{mod},\lambda} \sin^2 2(\phi - \theta_m) + I_\mathrm{b} \tag{1}$$

where

$$I_{\mathrm{mod},\lambda} = \frac{1}{\Delta\lambda} \int_{\lambda_\mathrm{lower}}^{\lambda_\mathrm{upper}} I_{p,\lambda} \sin^2(\delta_\lambda / 2)\, d\lambda \tag{2}$$

λ_upper and λ_lower denote the upper and lower limits of the wavelength in the spectrum of the light source, $\Delta\lambda = \lambda_\mathrm{upper} - \lambda_\mathrm{lower}$, $I_{\mathrm{p},\lambda}$ are the intensity coming out of the polariscope. ϕ is the isoclinic parameter or the angle of σ_1 with respect to the reference axis, θ_m is the phase-shifted angle at step m, and I_p is the total background intensity. δ_λ is the relative or fractional retardation relating to the principal stress difference ($\sigma_1 - \sigma_2$) in the plane stress state by the relation

$$\frac{\delta_\lambda}{2\pi} = N_\lambda = \frac{C_\lambda h}{\lambda}(\sigma_1 - \sigma_2) = \frac{h}{f_{\sigma,\lambda}}(\sigma_1 - \sigma_2) \tag{3}$$

where C_λ is the stress-optic coefficient, $f_{\sigma,\lambda}$ (= λ / C_λ) is the material stress fringe value obtained by calibration and h is the thickness of the model studied.

Elaborately manipulating to Eq. (2) with the identity $\sin^2(\gamma/2) = 1/2\,(1 - \cos\gamma)$, applying four-step phase shift method such that $\theta_m = \{(m - 1)\,\pi/8 \mid m = 1, 2, 3, 4\}$ and combining intensity equations obtained at each step for all three primary RGB wavelengths of white light, yields the following equation for determination of isoclinic parameter.

$$\phi_{\mathrm{w}} = \frac{\pi}{8} - \frac{1}{4}\arctan\left(\frac{I_1^{\mathrm{s}} - I_3^{\mathrm{s}}}{I_2^{\mathrm{s}} - I_4^{\mathrm{s}}}\right) \quad \text{for} \quad I_{\mathrm{mod}}^{\mathrm{s}} \neq 0 \tag{4}$$

where the subscript 'w' denotes the wrapped phase value. Note that,

$$I_m^{\mathrm{s}} = I_{m,\mathrm{R}}^{\mathrm{s}} + I_{m,\mathrm{G}}^{\mathrm{s}} + I_{m,\mathrm{B}}^{\mathrm{s}} \tag{5}$$

$$I_{\mathrm{mod}}^{\mathrm{s}} = \sqrt{(I_1^{\mathrm{s}} - I_3^{\mathrm{s}})^2 + (I_2^{\mathrm{s}} - I_4^{\mathrm{s}})^2} \tag{6}$$

$$I_{\mathrm{eff}}^{\mathrm{s}} = \frac{1}{4}(I_1^{\mathrm{s}} + I_3^{\mathrm{s}} + I_2^{\mathrm{s}} + I_4^{\mathrm{s}}) \tag{7}$$

The superscript 's' denotes a summation. It is important to be noted that before using Eq. (4), the summed value of I_m^{s} obtained from Eq. (5) should be normalized by a factor such that the summation does not exceed the maximum gray level used. Further, since ϕ is not a function of λ as shown in Eqs. (1) and (2); hence, Eqs. (4) to (7) are valid, i.e., integration of Eq. (2) is unnecessary.

2.2 Phase unwrapping

The PU algorithm already has been proposed [8]. Then, only its main processes are briefly described here. There are two main stages, i.e.,

- **Expansion Stage**: for a first place, the PU algorithm performs unwrapping starting from the initial region (largest region of the wrapped phase map of isoclinic parameter) by which the low-quality regions (the isotropic points and regions around them) are left. In this way, the errors in the low-quality regions are suppressed and the initial region continuously grows up along its boundary. It is in general that at the border of the specimen, the isoclinic angle values are unreliable. Thus, the use of pixels locating at and near the border as the seed point for unwrapping the wrapped pixels for the next loop may lead to errors in the unwrapped pixels and such errors may propagate to other pixels in the fringe field. Then, to prevent this, the PU algorithm is modified for isolating the pixels along the border such that they are unwrapped for a second place. For clarity, the PU algorithm firstly unwraps the wrapped pixels that are in the region of interest but not in the isolated region. After that, the wrapped pixels in the isolated region are processed.

- **Shrinkage Stage**: as a last place, upon completely finishing the expansion stage for both places, the PU algorithm continues performing starting from the boundaries of those left low-quality regions (especially the region of the isotropic points). These regions become smaller for each time of the process.

3. Experimental Setup and Results

The system used for recording the photoelastic fringe images is shown in Fig. 1. It mainly consists of a dark-field plane polariscope setup with a white light source (halogen lamp), a digital camera model SLR D70 of Nikon and a personal computer. The geometrical dimension and the direction of the applied load are shown in Fig. 2. All program code to perform the evaluation of the isoclinic parameter was implemented in VC++.

To further examine the performance of the method for the existence of the isotropic region, it was experimentally applied to the problem of the eccentrically loaded split ring (C-shaped model). The model was made of an epoxy resin plate. When performing the

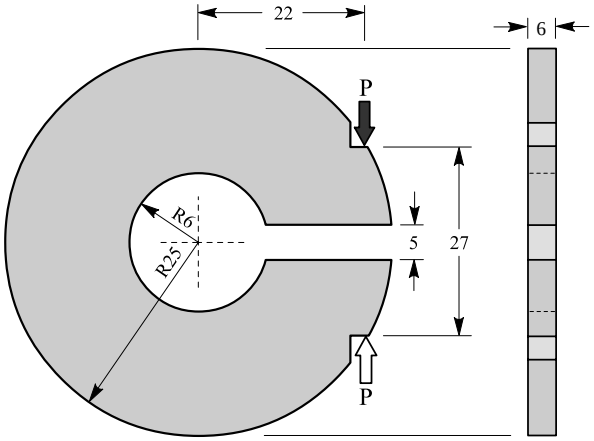

Fig. 2 Applied load direction and dimensions of the split ring under eccentrically compressive load P of 157 N. The black and white arrows indicate the applied load direction and the reaction at the supports, respectively. (Geometrical unit: mm and image not to scale)

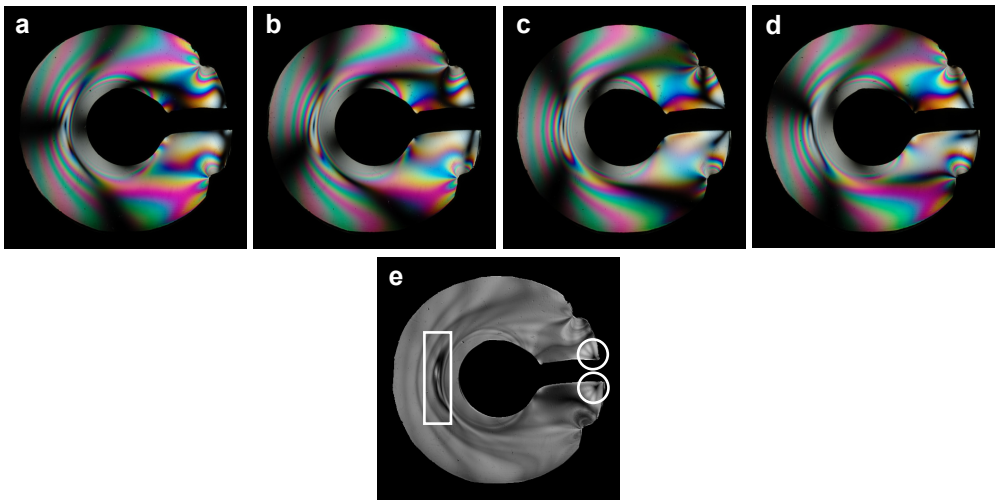

Fig. 3 Raw color photoelastic fringe images of the eccentrically loaded split ring with different setup of the polariscope system: (a) $\theta_1 = 0$, (b) $\theta_2 = +\pi/8$, (c) $\theta_3 = +\pi/4$, (d) $\theta_4 = +3\pi/8$ and (e) map of $I_{\text{mod}}^{\text{s}}$. The size of the images is 512 × 512 pixels. (Printed in black and white)

experiment, it was subjected to the eccentrically compressive load P = 157 N and then four photoelastic fringe images were digitally collected according to the four different orientations of the Polaroid's in the crossed combination.

The raw color fringe images of the model are in Figs. 3. The map of $I_{\text{mod}}^{\text{s}}$ is displayed in Fig. 3e. Figure 4 depicts the wrapped and unwrapped map of the isoclinic-angle values for different periods. The unwrapped map shown in Fig. 4c expresses the true range of $(-\pi/2, +\pi/2]$ of the isoclinic parameter. Note that all maps in Fig. 4 are generated from the maximum and minimum isoclinic angle values associated with their periods, i.e., the maximum value was represented by pure white whereas deep black represents the minimum value. Figure 5 displays the profile of the isoclinic-angle values along the red line as drawn in Fig. 4e and Fig. 6 shows the unwrapped map with several stress elements.

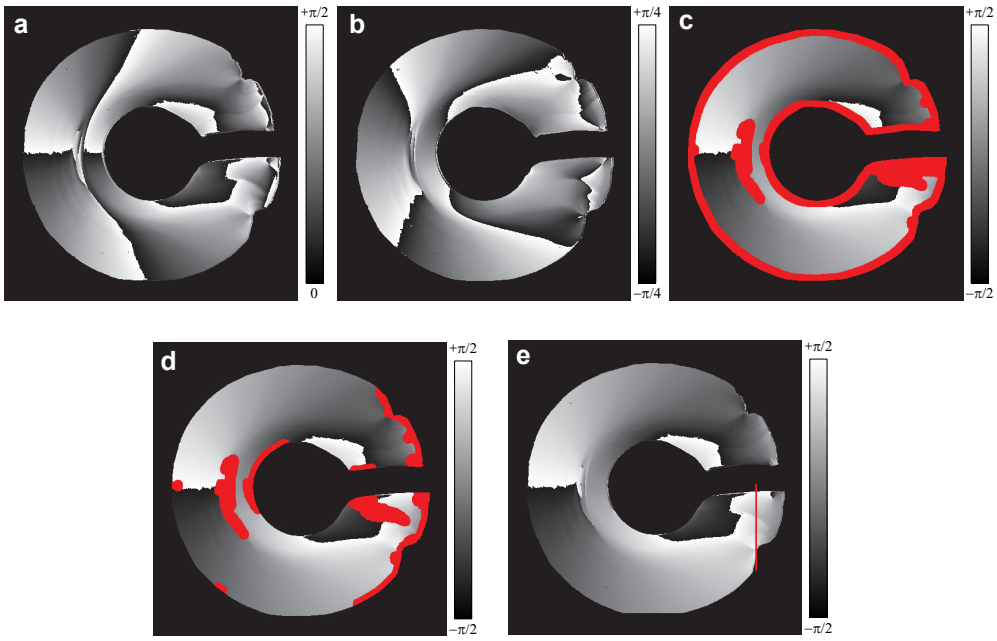

Fig. 4 Wrapped and unwrapped map of isoclinic-angle values: (a) wrapped map in the range of [0, + π/2], (b) wrapped map in the range of (−π/4, +π/4], (c) unwrapped map from the first place of the expansion stage, (d) unwrapped map from the second place of the expansion stage and (e) complete unwrapped map from the shrinkage stage in the range of (−π/2, +π/2]. (Printed in black and white)

4. Discussion

Using images shown in Figs. 3a -3d with Eq. (4) and the PU algorithm, the wrapped and unwrapped maps of the isoclinic-angle values are shown in Fig. 4. The wrapped maps in Fig. 4a and b are of the ranges of [0, +π/2] and (−π/4, +π/4], respectively. Figures 4c - 4e show the unwrapped map of the true range of (−π/2, +π/2].

Figures 4a and 4b were obtained from those isoclinic angle values, which were calculated using Eq. (4), by using the simple logic operations [8]. The unwrapped maps of the isoclinic-angle values obtained from the expansion stage are shown in Figs. 4c and 4d whereas Fig. 4e depicts the complete unwrapped map. The isolated region is shown in Fig. 4c as the red band around the shape of the model. This region was isolated by scanning over the mask image showing the region (ROI) occupied by the model using the 10 × 10 pixel-isolating window. Note further that there are other red regions in the map shown in Fig. 4d that are not the isolated region but they are of the isotropic points or regions (compare Fig. 4c with 4d).

After the isolated region was processed, the result rendered from the PU is shown in Fig. 4d. It is seen that there are several red regions that belong to both the isolated region and the isotropic points. The result of the shrinkage stage is shown in Fig. 4e. For Fig. 4e, the conditions $T_{\text{global}} = +0.8\pi/2$, $T_{\text{local}} = +0.4\pi/2$ and for the isotropic point detection $I^{s}_{\text{mod}} = 0.1I^{s}_{\text{mod,max}}$ were used in which T_{global} is the global threshold used to define the phase jumps in the fringe field, T_{local} is also the threshold but is used to define the phase jump for the isotropic point and $I^{s}_{\text{mod,max}}$ is the maximum values of I^{s}_{mod} (see Fig. 3e) [8]. Note that the size of window used to detect the isotropic points and to expand regions around such points was 21 × 21 pixels.

It is seen in Fig. 3e that there are two isotropic points (see circle marks) and one isotropic region (see rectangle). However, those two points in the circle marks are not the

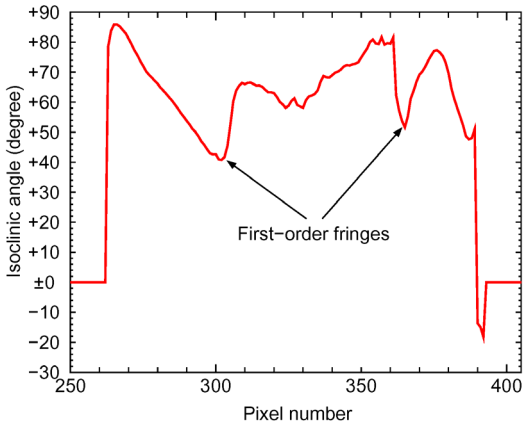

Fig. 5 Profile of the isoclinic-angle values along the (red) line as shown in Fig. 4e. This plot is to show the influence of the isochromatic parameter δ.

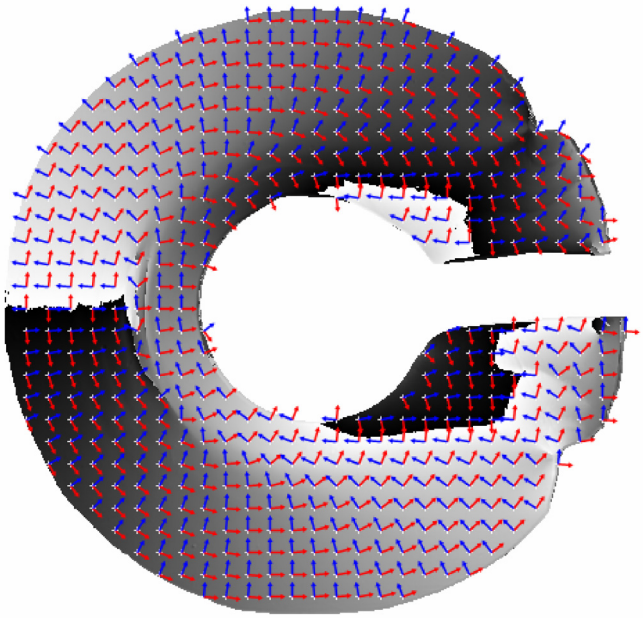

Fig. 6 Unwrapped map of the isoclinic-angle values in the interval $(-\pi/2,+\pi/2]$ with arrows indicating the isostatcis. Red arrow indicates σ_1 isostatics and blue arrow indicates σ_2 isostatics. (Printed in black and white)

isotropic point but they are the singular point because at the free edge the isochromatic parameter (fringe order) is zero (compare Fig. 3e with Fig. 4e). These points should be exactly on the free edges; however, the edge stress might force them to move toward inside. This can be confirmed by judiciously comparing with figure reported in Frocht's book [9]. Note that Fig. 4e was obtained by the combination of Figs. 4a and 4b [8].

One could see the effect of the isochromatic parameter, especially the first-order fringe in the isoclinic-angle map. The effect of the isochromatic parameter δ (at and near the load application points and the supports) in the isoclinic-angle map occurred because the distinction between the isoclinic fringe (black) and the first-order fringe (almost black) is difficult task. At that almost black region, I^{s}_{mod} approaches zero and the results obtained from Eq. (4) are unreliable. By this the unwrapped map is rather unsmooth.

Figure 5 shows the profile of the isoclinic-angle values along the red vertical line as

shown in Fig. 4e such that the influence of the isochromatic parameter is clearly observed; that is, the isoclinic-angle values are greatly reduced to some values associated with the degree of the closeness of I^{s}_{mod} to zero. The closer the I^{s}_{mod} to zero, the clearer the effect of the isochromatics. This effect can be seen by considering the condition in Eq. (4) ($I^{s}_{mod} \neq 0$). If I^{s}_{mod} approaches zero, the arctangent function returns the value almost equal to $+\pi/2$ or $-\pi/2$ depending on the net sign of its argument. It was found that at the 303th pixel, the net sign was of minus; therefore, the value of ϕ_w was forced toward to $+\pi/4$ regardless of the intensity values used.

Close consideration at the isotropic region (region in the rectangle in Fig. 3e) reveals that the isoclinic parameter gradually varies from $-\pi/2$ to $+\pi/2$ (from black to white) in the anticlockwise direction. Therefore, it is of the positive type [9]. The isoclinic-angle map can be used to identify one of the principle stress directions.

Figure 6 shows the unwrapped map with arrows indicating the directions of σ_1 and σ_2. This unwrapped map refers to the direction of σ_1 (red arrow). That is, if one connects the line between the points according to σ_2 direction (blue arrow), the connected lines represented the stress trajectories (isostatic) of σ_2 family (judiciously compare with figure reported in Ref. (9)). As one knows, there always exist two orthogonal principal stresses in the fringe field. The isostatic lines of σ_2, thus, verify that this unwrapped map represents the direction of σ_1.

5. Conclusion

In this paper, an extension of the PU algorithm for an automatic determination of the isoclinic parameter for the model possessing the isotropic region is presented. It is confirmed that the PU algorithm can render the unwrapped map of the isoclinic-angle values regardless of the presence of the isotropic region.

It was found that some points were assigned as the isotropic points in spite of the fact that they are not and this affected the processing time of the PU algorithm. Improvement of the isotropic point detection by combining the wrapped map as shown in Figs. 4a and 4b could offer higher accuracy for the isotropic point detection.

References

(1) Ramesh, K., Digital Photoelasticity: advanced techniques and applications, Springer, Berlin (2000), pp. 157, 231.
(2) Buckberry, C. and Towers, D., Opt. Lasers Eng., 24 (1996), pp. 415-428.
(3) Patterson, E.A. and Wang, Z.F., Strain, 27 (1991), pp. 49-56.
(4) Pinit, P. and Umezaki, E., Opt. Rev, 12 (2005), pp. 228-232.
(5) Nurse, A.D., Appl. Opt, 36 (1997), pp. 5781-5786.
(6) Plouzennec, N. and Lagarde, A., Exp. Mech, 39 (1999), pp. 274-277.
(7) Kihara, T., Strain, 39 (2003), pp. 65-71.
(8) Pinit, P. and Umezaki, E., Opt. Lasers Eng., 45 (2007), pp. 795-807
(9) Frocht, M.M., Photoelasticity, Vol. 1, New York, John Wiley_Sons (1941), pp. 194-195, 210-213.